Check for updates

Synthesis of stack plate covalent organic framework nanotubes using a self-assembled acid as a soft template†

Dan Wu,‡[ab] Dandan Han,‡[c] Yong Zhou,[a] Zhen Zhang,[b] Hang Qian,[b] Qian Zhou,[c] Yongsheng Zhang,[b] Andrei Y. Khodakov [ID] *[a] and Vitaly V. Ordomsky [ID] *[a]

COF-LZU1 with nanotube-like morphology has been synthesized with high crystallinity and pore volume in the presence of trimesic acid as a template. The as-synthesized COF nanotubes consist of a stack of plates with a diameter of about 100 nm with a hollow channel inside of about 20 nm.

Covalent organic frameworks (COFs) are kinds of purely organic crystalline materials with uniform pore size and tailored functional moieties.[1–4] Since the first introduction by Yaghi and co-workers in 2005,[5,6] COFs have been widely used in adsorption, separation, catalysis and electronics due to their ordered structure, high surface areas, low density, thermal and chemical stability, and easy functionalization.[7,8] In the past decade, a large number of COFs with different structures have been fabricated based on various covalent bonds (B–O, C–O, C–N, C=N, C=C, *etc.*).[9,10] Most of the research interest for COF synthesis focuses on tunable structures[11,12] and designable functionalities[13,14] to improve their physical and chemical properties. However, despite the benefits of tuning the structure and chemical functionalities of COFs, morphology-control of COFs, which is an extremely important factor in absorption and catalysis, is still a challenge due to the highly sensitive crystallization process.[15]

It is well known that COFs are synthesized by reversible dynamic covalent-bond formation.[16] A crystalline and ordered COF structure can only be constructed in a narrow synthetic window.[17] Such a trial-and-error synthetic process makes it

[a] Univ. Lille, CNRS, Centrale Lille, ENSCL, Univ. Artois, UMR 8181-UCCS-Unité de Catalyse et Chimie du Solide, F-59000 Lille, France.
E-mail: vitaly.ordomsky@univ-lille.fr, andrei.khodakov@univ-lille.fr
[b] School of Chemical Engineering, Zhengzhou University, Zhengzhou, 450001, People's Republic of China
[c] College of Science, Henan Agricultural University, Zhengzhou, Henan 450002, People's Republic of China

† Electronic supplementary information (ESI) available. See DOI: https://doi.org/10.1039/d2cc01735k

‡ These authors contributed equally to this work and should be considered co-first authors.

hard to control the morphologies of COFs during crystallization. Currently, there are only limited methods to tune the morphology of COFs without affecting the crystallinity. For example, a series of COF spheres, fibers and films could be obtained by the condensation of 1,3,5-benzenetricarbaldehyde (BTCA) and 1,3,5-tris(4-aminophenyl)benzene (TAPB) in the presence of a monofunctional amine and aldehyde added as competitors during the crystallization.[18] Besides, hollow tubular porous COFs have been synthesized by template-assisted replication of ZnO-nanorods,[19] while microtubular COFs can be synthesized from monomers consisting of diketopyrrolopyrrole (DPP) and tetraphenylporphyrin (TPP) moieties.[20] A two-step amorphous-to-crystalline strategy has also been well studied for the construction of different morphologies of COFs such as microspheres and fibers.[21,22] However, these strategies above either highly rely on the properties of the monomers or suffer from the use of costly hard templates and generally result in amorphous walls of COFs with overlapped or interconnected 2D layers. Thereby, a bottom-up strategy for the morphology-controlled synthesis of highly crystalline COFs regardless of the properties of the monomers is greatly desirable.

Herein, we present a novel facile strategy to control the morphology of COFs with well-defined crystalline walls. COF nanotubes have been synthesized by the condensation of 1,3,5-triformylbenzene (TFA) and *p*-phenylenediamine (PDA) in the presence of trimesic acid (TMA) under ambient conditions (Fig. 1a). Inter-molecular assemblies of TMA generate a rod-like soft template. *In situ* crystallization of COFs around the template leads to the formation of COF plates perpendicularly to the rods of TMA in the form of a nanotube. This work provides a general strategy for the synthesis of COF nanotubes with a well-defined structure of the walls, which would significantly extend the applications of COF materials.

First of all, COF-LZU1 has been synthesized following the conventional procedure *via* the condensation of TFA and PDA in dioxane solvent at room temperature.[23] In agreement with previous reports,[24] the obtained COF-LZU1 showed spherical
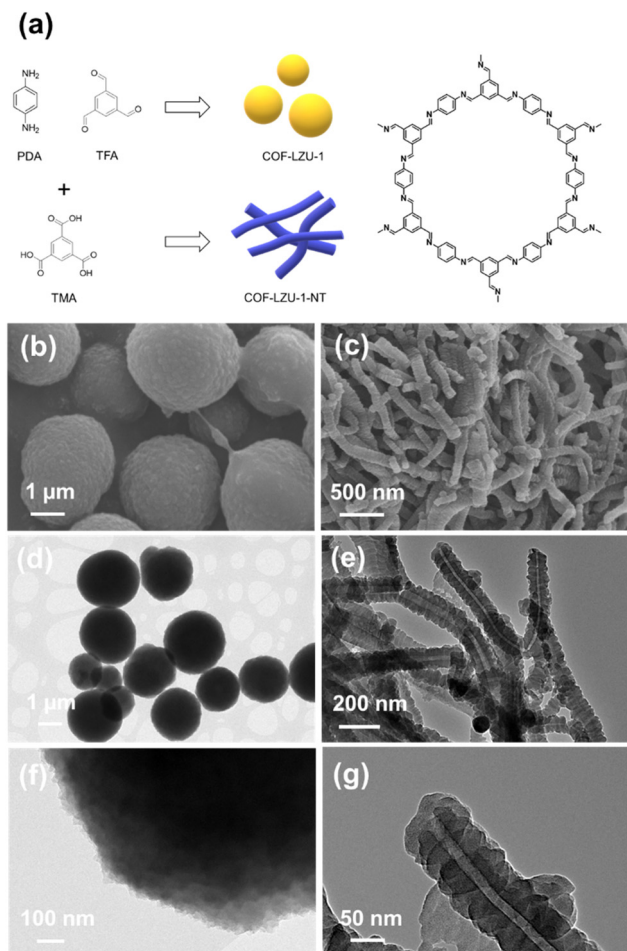
Fig. 1 Characterizations of COFs. (a) Illustration of the synthesis of conventional COF-LZU1 and COF-LZU1-NT; SEM images of (b) COF-LZU1 and (c) COF-LZU1-NT; TEM images of (d and f) COF-LZU1 and (e and g) COF-LZU1-NT.

Fig. 2 Characterizations of COF-LZU1 and COF-LZU1-NT. (a) XRD, (b) FTIR, (c) Raman, (d) ^{13}C solid-state NMR, (e) N$_2$ adsorption–desorption isotherms and corresponding (f) pore size distribution.

morphologies with an average particle size of around 2–4 μm (Fig. 1b, d and f). To control the morphology of COF-LZU1, TMA was introduced into the 1,4-dioxane solvent and co-crystallized with TFA and PDA. Surprisingly, a fiber-like morphology was fabricated as indicated by SEM analysis with a diameter of the fibers in the range of 100–200 nm (Fig. 1c). Further characterizations by transmission electron microscopy (TEM) analysis demonstrated an interesting structure of the material prepared in the presence of TMA (Fig. 1e) with stacked COF plates arranged perpendicularly to the hollow channel of about 20 nm in diameter (Fig. 1g).

The XRD analysis of both samples demonstrates typical COF-LZU1 structures with high crystallinity. The strongest peak at 4.7° arises from the (100) facet and a set of weak peaks at 8.2°, 9.4° and 12.7° corresponds to the (110), (200) and (210) facets, respectively (Fig. 2a).[25,26] The absence of (001) reflection corresponding to stacking between the layers in the XRD spectrum of COF-LZU1-NT is most probably due to the variation of the distances between the layers resulting in the broadening of the peak. The COF-LZU1 materials also show similar Fourier transform infrared (FTIR) spectra with a peak at 1615 cm^{-1}
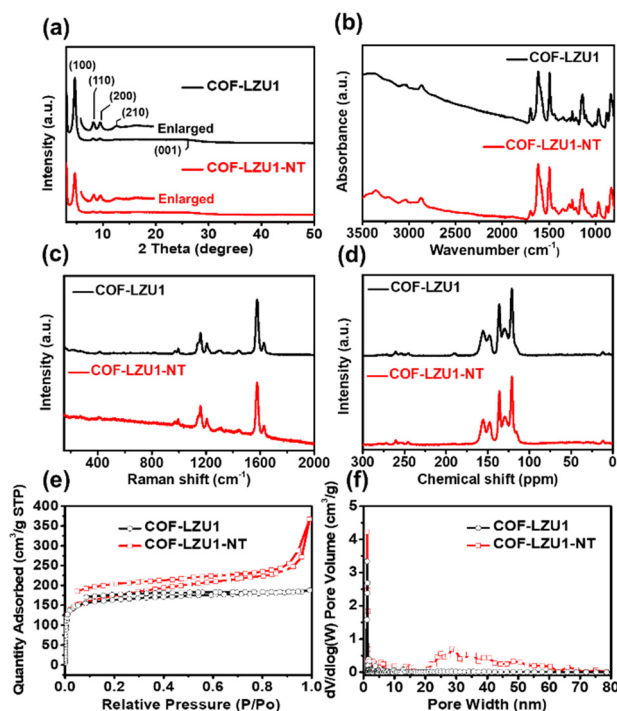
attributed to the C=N bond (Fig. 2b). Meanwhile, the intensity of the peak originating from the aldehyde group (1695 cm^{-1}) of TFA has decreased a lot (Fig. S1, ESI†), confirming the condensation of TFA and PDA.[23,25] A similar chemical structure is also confirmed by Raman spectroscopy (Fig. 2c). The absorption peak at 1624 cm^{-1} was attributed to the C=N stretching vibration in the linkages.[27] The adsorption peaks at 1578, 1158, and 992 cm^{-1} were assigned to C=C stretching, C–H bending and C–H plane deformation in the benzene ring, respectively.[27] Solid–state cross-polarization magic-angle spinning ^{13}C nuclear magnetic resonance (^{13}C CP/MAS NMR) was used to check the chemical environment of both samples (Fig. 2d). The ^{13}C NMR peak at ∼156 ppm corresponds to the C atom of the C=N bonds, confirming the condensation of TFA and PDA. A set of resonance peaks at ∼148, ∼136, ∼130, and ∼121 ppm can be attributed to the carbon atoms of the phenyl groups.[28,29] The minor resonance at ∼189 ppm is assigned to the carbon atom of C=O bonds in the terminal TFA moieties.[25] The chemical analysis also shows similar N, H, C and O contents for both samples (Table 1). A slightly higher O content in COF-LZU1-NT could be ascribed to the residual TMA molecules inside the COF nanotubes. Thus, the characterization techniques indicate the similar chemical structure of the COF nanotubes and the conventional COF-LZU1 materials. This means that the addition of TMA mostly changes the morphology of the COFs with no effect on the composition and structure.

The information obtained from the N$_2$ adsorption–desorption isotherms also pointed to the different sample morphology. As shown in Fig. 2e, COF-LZU1 exhibits a type I isotherm of N$_2$

Table 1 Characterization of the as-synthesized COF-LZU1 and COF-LZU1-NT

Samples	S_{BET} (m^2 g^{-1})	V_{micro} (cm^3 g^{-1})	V_{meso} (cm^3 g^{-1})	Elemental analysis (%)			
				C	H	N	O
COF-LZU1	508	0.23	0.04	76.3	4.6	14.5	4.5
COF-LZU1-NT	560	0.22	0.31	74.5	4.7	14.5	6.2

with a steep increase in adsorption below $p/p_o = 0.1$ suggesting the presence of intrinsic micropores of COF-LZU1.[25] Interestingly, different from COF-LZU1, an obvious N$_2$ uptake at $p/p_o > 0.8$ was observed in COF-LZU1-NT corresponding to the Type II IUPAC classification typical for CNTs.[30] This phenomenon is attributed to the capillary condensation of N$_2$ in the channels of the COF nanotubes, in agreement with TEM analysis.[31,32] The Brunauer–Emmett–Teller (BET) surface areas were calculated to be 508 m^2 g^{-1} for COF-LZU1 and 560 m^2 g^{-1} for COF-LZU1-NT (Table 1). The slightly higher BET surface area of COF-LZU1-NT could be ascribed to the presence of voids inside the nanotubes.[33] The cumulative pore volume of both samples was calculated by nonlocal density functional theory (NLDFT) and both samples show a similar pore volume for the micropores (0.23 *vs.* 0.22 cm^3 g^{-1}). However, COF-LZU1-NT exhibited a much higher mesoporous volume than COF-LZU1 (Table 1, 0.31 *vs.* 0.04 m^3 g^{-1}). The pore size distribution shown in Fig. 2f demonstrates the presence of mesopores in the range of 20–60 nm in COF-LZU1-NT in agreement with TEM analysis (Fig. 1f).

The thermal stability of COF-LZU1-NT was checked by thermal gravimetric (TG) analysis. As shown in Fig. S2 (ESI†), both COF-LZU1 and COF-LZU1-NT showed good thermal stability (up to 350 °C), which agrees with the literature.[25] Notably, after calcination at 250 °C for 1 h, the crystal structure and morphologies of COF-LZU1-NT did not change (Fig. S3, ESI†). The chemical stability of the as-synthesized COF-LZU1-NT has been examined by stirring the material in 1 M HCl and 1 M NaOH for 24 h. COF-LZU1-NT demonstrates preservation of the structure in a base (NaOH) and decomposition in the presence of an acid (HCl, Fig. S4, ESI†).

It has been recently reported that TMA can form fiber-like self-assemblies in the THF solvent.[34] Thus, the addition of TMA in the solvent was expected to act as a soft template for regulating the growth of COFs. In order to confirm the role of TMA in the formation of COF nanotubes, pure TMA was firstly dissolved in dioxane and drop-cast on a copper grid for SEM and TEM analysis. As shown in Fig. S5 (ESI†) and Fig. 3b, a rod-like morphology of TMA self-assemblies was formed, demonstrating the feasibility of the TMA template for directing the growth of COF nanotubes. The acid sites of TMA oriented perpendicularly to the rods could act as nucleation sites for the crystallization of COF plates. The formation of the COF nanotubes was illustrated in Fig. 3a. Firstly, a rod-like TMA assembly was generated as a soft template (Fig. 3b). Then, the COF precursors of TFA and PDA encircle the TMA rods. This phenomenon is also confirmed by TEM (Fig. 3c). The presence of the TMA template inside the COF nanotubes was also
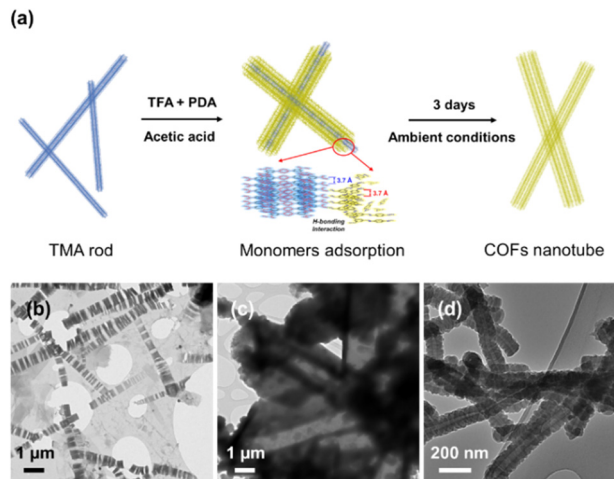
Fig. 3 Mechanistic studies of COF nanotube formation. (a) Schematic for the formation of COF nanotubes; TEM analysis for (b) trimesic acid, (c) intermediate at the initial time, and (d) COF nanotubes.

confirmed by the XRD and FTIR analysis of the sample before washing (Fig. S6 and S7, ESI†). Hydrogen-bonding between –COOH (TMA) and –NH$_2$ (PDA) and –C═O (TFA) results in the condensation of COF monomers perpendicular to the TMA rod. For example, the use of a heteropolyacid in the crystallization of COF has been reported earlier.[35] The removal of TMA by washing leads to the generation of the void space inside of the nanotubes (Fig. 3d). It is worth mentioning that the layer distance between the TMA nanorods has been reported to be 3.7 Å,[34] which corresponds to the layer distance of COF-LZU1 (Fig. 3a).[25] The layer distance matching could be the possible reason for the crystalline COF wall formation.

Different solvents and reaction temperatures resulted in insufficient COF formation (Fig. S8, ESI†). These results indicate that the formation of COF nanotubes is highly dependent on the reaction conditions. This can be attributed to the sensitivity of TMA morphology and interaction with monomers as function of the reaction conditions.

Furthermore, the synthesized COF nanotubes were further used as an oil adsorbent for the removal of oil contamination from water. The adsorption of relatively large molecules present in the oils is facilitated by the hierarchical structure of the COF nanotubes containing both micropores and mesopores. As shown in Fig. 4a, COF-LZU1-NT shows a lower density than COF-LZU1 (0.08 *vs.* 0.56 g cm^{-3}). This difference could be ascribed to the abundance of voids inside the nanotubes. As shown in Fig. 4c, five common oils of different origins have been selected for the adsorption tests. The adsorption capacity of COF-LZU1-NT is much higher than that of COF-LZU1 for all the oils. While initial COF-LZU1 absorbed the amount of oil corresponding to its pore volume (Table 1), COF-LZU1-NT can adsorb a 3-times higher amount. In comparison with the conventional strategy of making COF coatings on melanin foams,[36] we demonstrate here that morphology-controlled synthesis of hierarchical COF nanotubes is an efficient way to enhance the adsorption capacity of COF materials. This kind of enhancement could be
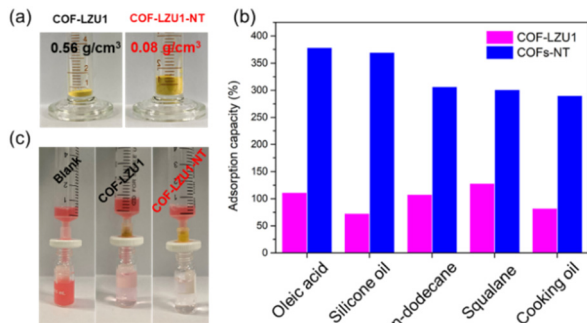
Fig. 4 Adsorption of oils by COFs. (a) The apparent density of COF-LZU1 and COF-LZU1-NT; (b) adsorption capacity (%) of various oils by COF-LZU1 and COF-LZU1-NT; (c) filtration of oil microdroplets from water by COF-LZU1 and COF-LZU1-NT.

ascribed to the abundant voids inside the COF nanotubes, which act as the reservoir to accommodate more oils. Furthermore, we applied COF-LZU1 and COF-LZU1-NT in the adsorption of an oil-in-water emulsion by filtration. As shown in Fig. 4c, COF-LZU1-NT shows obvious efficiency for absorption of oil in the water compared to COF-LZU1. Moreover, the filtrate has been weighed and analyzed by gas chromatography. Specifically, when 3 g of the oil-in-water emulsion was used, the amount of oleic acid in the filtrate was only 3.3 mg for COF-LZU1-NT, while 18 mg for COF-LZU1, demonstrating the high oil adsorption selectivity of COF-LZU1-NT. It is worth mentioning that the absorption of oil droplets in the water demands the adsorbent to possess not only high adsorption capacity but also high selectivity for oils. As confirmed by water contact angle (CA) measurement (Fig. S9, ESI†), the COF-LZU1-NT has an increased CA compared to the initial COF-LZU1 (91° *vs.* 64°), thus ensuring a higher selectivity to oil adsorption than water.

We demonstrated here a general strategy for the morphology-control of COFs and synthesis of hierarchical micro and meso-porous COF nanotubes with a well-defined crystalline wall structure. The utilization of trimesic acid as a soft template has been proposed as an effective way to regulate the morphology of COFs. The formation of trimesic acid rod-like templates and adsorption and growth of COFs around the template lead to the unique nanotube morphology of stacked plates. The abundant meso-porous voids in the hollow channels within COF nanotubes endow the materials with high capacity for adsorption of oily contamination from water. This work affords an alternative way to improve the pore volume and diffusion properties of COF materials, which would significantly promote their further applications in separation, adsorption, and catalysis using relatively large molecules.

The manuscript was written with the contributions of all authors. All authors have given approval to the final version of the manuscript.

Conflicts of interest

There are no conflicts to declare.

Notes and references

1 S. Das, P. Heasman, T. Ben and S. Qiu, *Chem. Rev.*, 2017, **117**, 1515–1563.
2 N. Huang, P. Wang and D. Jiang, *Nat. Rev. Mater.*, 2016, **1**, 16068.
3 A. G. Slater and A. I. Cooper, *Science*, 2015, **348**, aaa8075.
4 X. Feng, X. Ding and D. Jiang, *Chem. Soc. Rev.*, 2012, **41**, 6010–6022.
5 A. P. Cote, A. I. Benin, N. W. Ockwig, M. O'Keeffe, A. J. Matzger and O. M. Yaghi, *Science*, 2005, **310**, 1166–1170.
6 C. S. Diercks and O. M. Yaghi, *Science*, 2017, **355**, eaal1585.
7 P. Poizot, J. Gaubicher, S. Renault, L. Dubois, Y. Liang and Y. Yao, *Chem. Rev.*, 2020, **120**, 6490–6557.
8 Z. Wang, S. Zhang, Y. Chen, Z. Zhang and S. Ma, *Chem. Soc. Rev.*, 2020, **49**, 708–735.
9 S. Kandambeth, K. Dey and R. Banerjee, *J. Am. Chem. Soc.*, 2019, **141**, 1807–1822.
10 P. J. Waller, F. Gandara and O. M. Yaghi, *Acc. Chem. Res.*, 2015, **48**, 3053–3063.
11 S. Cao, B. Li, R. Zhu and H. Pang, *Chem. Eng. J.*, 2019, **355**, 602–623.
12 Y. Song, Q. Sun, B. Aguila and S. Ma, *Adv. Sci.*, 2019, **6**, 1801410.
13 K. Geng, T. He, R. Liu, S. Dalapati, K. T. Tan, Z. Li, S. Tao, Y. Gong, Q. Jiang and D. Jiang, *Chem. Rev.*, 2020, **120**, 8814–8933.
14 J. L. Segura, S. Royuela and M. Mar Ramos, *Chem. Soc. Rev.*, 2019, **48**, 3903–3945.
15 S. Kandambeth, V. Venkatesh, D. B. Shinde, S. Kumari, A. Halder, S. Verma and R. Banerjee, *Nat. Commun.*, 2015, **6**, 6786.
16 R. K. Sharma, P. Yadav, M. Yadav, R. Gupta, P. Rana, A. Srivastava, R. Zbořil, R. S. Varma, M. Antonietti and M. B. Gawande, *Mater. Horiz.*, 2020, **7**, 411–454.
17 T. Ma, L. Wei, L. Liang, S. Yin, L. Xu, J. Niu, H. Xue, X. Wang, J. Sun, Y. B. Zhang and W. Wang, *Nat. Commun.*, 2020, **11**, 6128.
18 S. Wang, Z. Zhang, H. Zhang, A. G. Rajan, N. Xu, Y. Yang, Y. Zeng, P. Liu, X. Zhang, Q. Mao, Y. He, J. Zhao, B.-G. Li, M. S. Strano and W.-J. Wang, *Matter*, 2019, **1**, 1592–1605.
19 P. Pachfule, S. Kandmabeth, A. Mallick and R. Banerjee, *Chem. Commun.*, 2015, **51**, 11717–11720.
20 B. Gole, V. Stepanenko, S. Rager, M. Grune, D. D. Medina, T. Bein, F. Wurthner and F. Beuerle, *Angew. Chem., Int. Ed.*, 2018, **57**, 846–850.
21 J. Tan, S. Namuangruk, W. Kong, N. Kungwan, J. Guo and C. Wang, *Angew. Chem., Int. Ed.*, 2016, **55**, 13979–13984.
22 W. Kong, W. Jia, R. Wang, Y. Gong, C. Wang, P. Wu and J. Guo, *Chem. Commun.*, 2019, **55**, 75–78.
23 Y. Peng, W. K. Wong, Z. Hu, Y. Cheng, D. Yuan, S. A. Khan and D. Zhao, *Chem. Mater.*, 2016, **28**, 5095–5101.
24 S. Hao, S. Li and Z. Jia, *J. Nanopart. Res.*, 2020, **22**, 270.
25 S. Y. Ding, J. Gao, Q. Wang, Y. Zhang, W. G. Song, C. Y. Su and W. Wang, *J. Am. Chem. Soc.*, 2011, **133**, 19816–19822.
26 H. Fan, H. Peng, I. Strauss, A. Mundstock, H. Meng and J. Caro, *J. Am. Chem. Soc.*, 2020, **142**, 6872–6877.
27 T. Jadhav, Y. Fang, W. Patterson, C. H. Liu, E. Hamzehpoor and D. F. Perepichka, *Angew. Chem., Int. Ed.*, 2019, **58**, 13753–13757.
28 S. Y. Ding, X. H. Cui, J. Feng, G. Lu and W. Wang, *Chem. Commun.*, 2017, **53**, 11956–11959.
29 Y. Li, Q. Wu, X. Guo, M. Zhang, B. Chen, G. Wei, X. Li, X. Li, S. Li and L. Ma, *Nat. Commun.*, 2020, **11**, 599.
30 X. Gu, W. Qi, X. Xu, Z. Sun, L. Zhang, W. Liu, X. Pan and D. Su, *Nanoscale*, 2014, **6**, 6609–6616.
31 M. Kruk and M. Jaroniec, *Chem. Mater.*, 2001, **13**, 3169–3183.
32 M. Thommes, K. Kaneko, A. V. Neimark, J. P. Olivier, F. Rodriguez-Reinoso, J. Rouquerol and K. S. W. Sing, *Pure Appl. Chem.*, 2015, **87**, 1051–1069.
33 B. P. Biswal, S. Chandra, S. Kandambeth, B. Lukose, T. Heine and R. Banerjee, *J. Am. Chem. Soc.*, 2013, **135**, 5328–5331.
34 S. Tothadi, K. Koner, K. Dey, M. Addicoat and R. Banerjee, *ACS Appl. Mater. Interfaces*, 2020, **12**, 15588–15594.
35 T. Gao, Z. Yan, V. Ordomsky and S. Paul, *ChemCatChem*, 2022, DOI: **10.1002/cctc.202101450**.
36 Q. Sun, B. Aguila, J. A. Perman, T. Butts, F.-S. Xiao and S. Ma, *Chem*, 2018, **4**, 1726–1739.